

# Slicing Pomerons in ultraperipheral collisions using forward neutrons from nuclear breakup

M. Alvioli,<sup>1,2</sup> V. Guzey,<sup>3</sup> and M. Strikman<sup>4</sup>

<sup>1</sup>*Consiglio Nazionale delle Ricerche, Istituto di Ricerca per la Protezione Idrogeologica, via Madonna Alta 126, I-06128, Perugia, Italy*

<sup>2</sup>*Istituto Nazionale di Fisica Nucleare, Sezione di Perugia, via Pascoli 23c, I-06123, Perugia, Italy*

<sup>3</sup>*University of Jyväskylä, Department of Physics, P.O. Box 35, FI-40014 University of Jyväskylä, Finland and Helsinki Institute of Physics, P.O. Box 64, FI-00014 University of Helsinki, Finland*

<sup>4</sup>*Pennsylvania State University, University Park, PA, 16802, USA*

(Dated: July 3, 2024)

We argue that measurements of forward neutrons from nuclear breakup in inclusive high energy photon-nucleus ( $\gamma A$ ) scattering provide a novel way to study small- $x$  dynamics of QCD in heavy-ion ultraperipheral collisions (UPCs). Using models for hadronic fluctuations of the real photon and neutron emission in nuclear fragmentation, we calculate the distribution over the number of evaporation neutrons produced in  $\gamma Pb$  collisions at the LHC. We show that it is correlated with the number of wounded nucleons (inelastic collisions) and, hence, can constrain the mechanism of nuclear shadowing and its  $x$  dependence.

PACS numbers:

Keywords: Heavy-ion scattering, ultraperipheral collisions, nuclear shadowing

## I. INTRODUCTION AND MOTIVATION

Understanding of the QCD dynamics of hard high energy interactions and the structure of nuclei and nucleons is one of the main directions of theoretical and experimental studies at the Large Hadron Collider (LHC) and the Relativistic Heavy Ion Collider (RHIC). Of particular interest is the limit of very small momentum fractions  $x$ , when the linear Dokshitzer-Gribov-Lipatov-Altarelli-Parisi (DGLAP) approximation is expected to break down [1, 2] and a regime close to the black disk limit (BDL) [3] may set in. Its observation is one of the prime objectives of the planned Electron-Ion Collider (EIC) at Brookhaven National Laboratory [4, 5], which will ultimately reach  $x \sim 10^{-3}$  for momentum transfers of a few GeV. At the same time, it was pointed out some time ago that ultraperipheral collisions (UPCs) of two ions at the LHC, where a photon emitted by one of the nuclei interacts with the other nucleus, allow one to probe down to  $x \sim 10^{-5} - 10^{-4}$ , depending on a particular reaction channel and the detector geometry [6, 7].

Electron-nucleus collisions at the EIC and UPCs of heavy ions at the LHC present two options for studying small- $x$  dynamics, which are largely complementary. At the LHC practically all data are collected for one heavy nucleus and one cannot directly access the dependence of cross sections on the virtuality of the probe. At the same time, one can reach very small  $x$ , which is provided by a wide rapidity coverage of the LHC detectors and the large invariant photon-nucleus collision energies exceeding by a factor of 100 the design energies at the EIC.

Over the last decade the data taken in the LHC and RHIC kinematics discovered a significant nuclear suppression of coherent  $J/\psi$  photoproduction in Pb-Pb and Au-Au UPCs compared to the impulse approximation prediction [8]. When interpreted in the leading twist approximation (LTA) [9], it amounts to strong gluon nuclear shadowing [10, 11]:

$$R_A^g(x, Q^2) = \frac{g_A(x, Q^2)}{Ag_N(x, Q^2)} < 1, \quad (1)$$

where  $g_A(x, Q^2)$  and  $g_N(x, Q^2)$  are the nucleus and nucleon gluon densities, respectively. Typical numbers reported by the LHC experiments, see [8] for references, correspond to

$$\begin{aligned} R_{\text{Pb}}^g(x = 10^{-3}, Q_{\text{eff}}^2 = 3 \text{ GeV}^2) &\approx 0.6, \\ R_{\text{Pb}}^g(x = 10^{-4}, Q_{\text{eff}}^2 = 3 \text{ GeV}^2) &\approx 0.5, \end{aligned} \quad (2)$$

with a similar suppression extending down to  $x \sim 10^{-5}$ . Here  $Q_{\text{eff}}$  is the effective resolution scale determined by the charm quark mass. These values of  $R_{\text{Pb}}^g$  agree very well with the LTA predictions for nuclear shadowing made more than 10 years ago [9]. Note that this interpretation of the  $J/\psi$  UPC data is complicated at the next-to-leading order (NLO) of the perturbative expansion in powers of  $\log Q^2$  (perturbative QCD) due to large cancellations between the leading-order (LO) and NLO gluon terms and a numerically important quark contribution [12, 13]. A way to stabilize the perturbation series and restore the gluon dominance in this process on the proton target was suggested in [14, 15].

Other hard UPC processes considered in the literature are inclusive [6, 16] and diffractive [17] dijet photoproduction, which are still to produce final results [18, 19], timelike Compton scattering [20–22], and heavy quark photoproduction [23–25]. Overall these findings confirm the conclusion of [7] that UPCs provide a very effective tool to access the small- $x$  dynamics of the strong interactions and the nuclear structure in hard, semi-hard and soft regimes of QCD.

So far the experimental studies of UPCs have mainly been focusing on coherent and incoherent production of light and heavy vector mesons. In this paper, we would like to outline several possible directions of future UPC studies, which were not discussed in the review [7] due to the lack of experimental confirmations of large nuclear shadowing. We explore for the first time possibilities of testing the small- $x$  nuclear shadowing dynamics by measuring the rates of forward neutron production from nuclear breakup in the zero degree calorimeters (ZDCs) at the LHC. Our numerical studies demonstrate that the number of produced neutrons is correlated with the number of wounded nucleons (inelastic photon-nucleon interactions), which presents a complementary way to study the mechanism of nuclear shadowing. In particular, as follows from the title of this paper, it allows one to control the number of unitarity cuts of diffractive exchanges (Pomerons), which build up the effect of nuclear shadowing.

This paper is organized as follows. In Sec. II we briefly summarize expectations based on applications of the Abramovski-Gribov-Kancheli (AGK) theorem to photon-nucleus scattering, model the distribution over the number of wounded nucleons and estimate its average value in the current UPC kinematics. Section III presents our predictions for the distributions over the number of emitted forward neutrons from nuclear breakup in inelastic photon-nucleus scattering. Our conclusions and outlook are given Sec. IV.

## II. ABRAMOVSKI-GRIBOV-KANCHELI (AGK) CUTTING RULES, NUCLEAR SHADOWING AND THE NUMBER OF WOUNDED NUCLEONS IN $\gamma A$ SCATTERING

Part of the results discussed in this section have been presented in [26]; we summarize them below for completeness since they are needed for new results in Sec. III.

It was demonstrated by Abramovski, Gribov and Kancheli in 1973 [27] that different unitary cuts of the diagrams corresponding to multi-Pomeron (color singlet) exchanges result in different multiplicities of produced particles in the central rapidity region and that the absorptive part of the amplitude can be expressed in terms of a small number of cut diagrams. They are related by combinatorial factors, which is known as the Abramovski-Gribov-Kancheli (AGK) cutting rules or the AGK cancellation. For the interpretation of the AGK rules in QCD and other effective field theories, see Refs. [28–32].

The application of the AGK cutting rules to photon-nucleus scattering allows one to express the nuclear shadowing correction to the total nuclear cross section  $\sigma_{\text{tot}}^{\gamma A}$  in terms of the diffractive cross section on individual nucleons [9, 33].

Another important application of the AGK cutting rules involves the total hadron-nucleus inelastic cross section defined as the difference between the total and total elastic (coherent plus incoherent) cross sections, which is obtained using the unitary form of the Glauber theory [34]. Generalizing this result to photon-nucleus scattering by taking into account that the photon takes part in the strong interactions by means of its hadronic fluctuations, the photon-nucleus total inelastic cross section can be presented in the following form [26]

$$\sigma_{\text{inel}}^{\gamma A} = \sum_{\nu=1}^A \sigma_{\nu}, \quad (3)$$

where

$$\sigma_{\nu} = \frac{A!}{(A-\nu)! \nu!} \int d^2 \vec{b} \int d\sigma P_{\gamma}(\sigma) (\sigma_{\text{inel}} T_A(\vec{b}))^{\nu} (1 - \sigma_{\text{inel}} T_A(\vec{b}))^{A-\nu}. \quad (4)$$

In Eq. (4),  $\vec{b}$  is the impact parameter (transverse coordinate) of the interacting nucleon,  $T_A(\vec{b}) = \int dz \rho_A(\vec{b}, z)$ , where  $\rho_A(\vec{b}, z)$  is the nuclear density normalized to unity, and  $\sigma_{\text{inel}} = 0.85 \sigma$  is the inelastic cross section for the interaction of a hadronic fluctuation of the photon with a target nucleon, which is based on the estimate that the  $\rho$  meson-nucleon elastic cross section constitutes approximately 15% of the total one. The cross sections  $\sigma_{\nu}$  in Eqs. (3) and (4) represent the physical process, where  $\nu$  nucleons undergo inelastic scattering, while the remaining  $A - \nu$  nucleons provide absorption. In the literature, one uses the term “wounded nucleons” [35] and the notation  $\nu = N_{\text{coll}}$ .

The distribution  $P_{\gamma}(\sigma)$  gives the probability density for hadronic fluctuations of the real photon to interact with nucleons with the cross section  $\sigma$  [26, 36]. While the shape of  $P_{\gamma}(\sigma)$  cannot be calculated from the first principles, one can reliably model it using constraints on its first moments and the small- $\sigma$  and large- $\sigma$  limits. Indeed, the total photon-proton cross section  $\sigma_{\gamma p}(W)$  and the cross section of photon diffractive dissociation on the proton

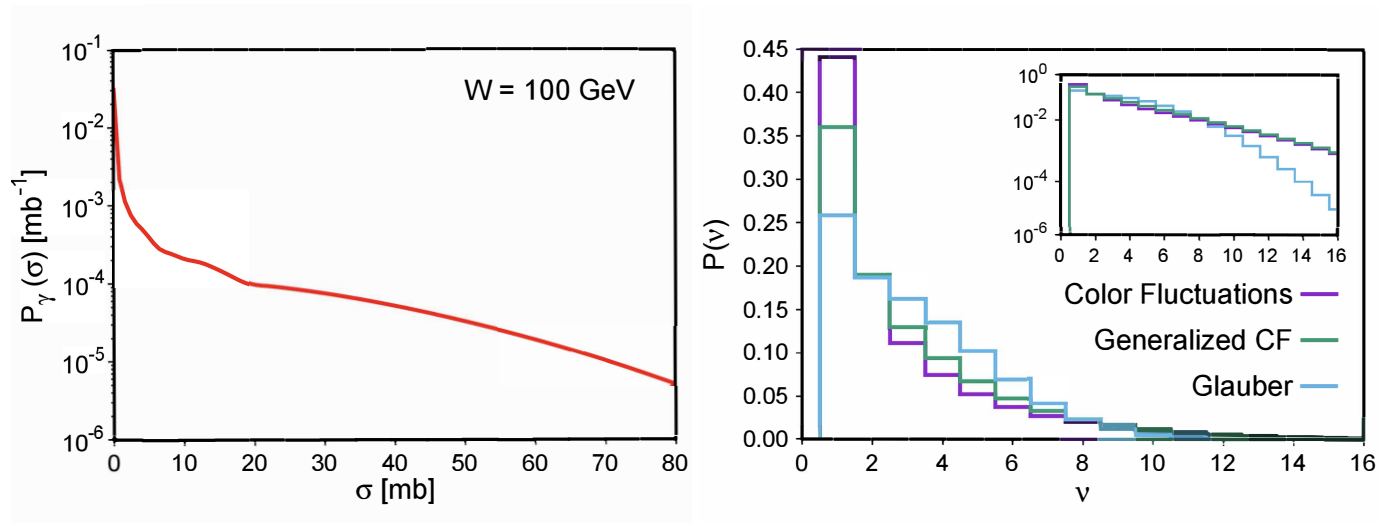


FIG. 1: (Left) The probability density  $P_\gamma(\sigma)$  for hadronic fluctuations of the real photon to interact with nucleons with the cross section  $\sigma$  at  $W = 100$  GeV. (Right) The  $P(\nu)$  distribution over the number of wounded nucleons (inelastic interactions)  $\nu$  in inelastic photon-nucleus (Pb) scattering. The three curves correspond to the three models for  $P_\gamma(\sigma)$ , see text for details. The insert emphasizes the region of large  $\nu$ . The figures are adopted from [26].

$d\sigma_{\gamma p \rightarrow Xp}(W, t=0)/dt$  constrain the first two moments of  $P_\gamma(\sigma)$  as follows

$$\begin{aligned} \sigma_{\gamma p}(W) &= \int d\sigma P_\gamma(\sigma) \sigma, \\ \frac{d\sigma_{\gamma p}(W, t=0)}{dt} &= \frac{1}{16\pi} \int d\sigma P_\gamma(\sigma) \sigma^2, \end{aligned} \quad (5)$$

where  $W$  is the invariant photon-nucleon center-of-mass-energy. Further, in the small- $\sigma$  limit, one can express  $P_\gamma(\sigma)$  in terms of the quark-antiquark component of the photon light-cone wave function and the color dipole cross section, which results in  $P_\gamma(\sigma) \propto 1/\sigma$ . In the opposite limit of large  $\sigma$ , the photon behaves as a superposition of the  $\rho$ ,  $\omega$  and  $\phi$  vector mesons in the spirit of the vector meson dominance model and, hence,  $P_\gamma(\sigma)$  can be modeled using hadronic (cross section) fluctuations in  $\rho$  mesons, which in turn are related to those for pions. Finally, the small- $\sigma$  and large- $\sigma$  regimes can be smoothly interpolated. Note that this matching is achieved best, when the light quark masses  $m_q$  are taken to be those of the constituent quarks,  $m_q \sim 300$  MeV. For details, see [26, 36].

The left panel of Fig. 1 presents the resulting distribution  $P_\gamma(\sigma)$  as a function of  $\sigma$  at  $W = 100$  GeV. Its shape and normalization are constrained by the procedure outlined above, the parametrization of  $\sigma_{\gamma p}(W)$  [37], and the data on  $d\sigma_{\gamma p \rightarrow Xp}(W, t=0)/dt$  [38]. Since the  $W$  dependence of  $P_\gamma(\sigma)$  is weak, the presented distribution is applicable to a wide range of energies probed in heavy-ion UPCs at the LHC. Note that the distribution  $P_\gamma(\sigma)$  parametrizes the so-called resolved photon contribution to photon-induced scattering and does not contain the direct photon contribution.

Note that the notion of cross section (color) fluctuations in hadron-nucleus scattering has found important phenomenological applications and confirmation in jet production in proton-nucleus scattering at the LHC and deuteron-nucleus scattering at RHIC [39, 40] as well as in pion and photon production in  $d + \text{Au}$  scattering at RHIC [41].

Using Eqs. (3) and (4), one can readily define the  $P(\nu)$  probability distribution for the number of wounded nucleons  $\nu$  in inelastic photon-nucleus scattering as follows [26],

$$P(\nu) = \frac{\sigma_\nu}{\sum_{\nu=1}^A \sigma_\nu}, \quad (6)$$

where  $\sigma_\nu$  is given by Eq. (4). To calculate it, we use the Monte Carlo generator for nucleon configurations in complex nuclei [42], which also includes nucleon-nucleon correlations in the nucleus wave function [43, 44], and the Gribov-Glauber model for photon-nucleus scattering, where the hadronic structure of the photon is described by  $P_\gamma(\sigma)$ . The resulting distribution  $P(\nu)$  as a function of  $\nu$  for lead (Pb) is shown by the curve labeled “Color Fluctuations” in the right panel of Fig. 1.

Our modeling of small- $\sigma$  hadronic fluctuations of the photon is based on the quark-antiquark component of the photon wave function and corresponds to a weak nuclear shadowing, which disagrees with the observed strong gluon

nuclear shadowing, see Eq. (2). To take it into account, we model the nuclear suppression of the dipoles with  $\sigma \leq \sigma_0 = 20$  mb by the factor of  $R_A^g$ , which leads to the modified distribution  $\tilde{P}_\gamma(\sigma)$ ,

$$\tilde{P}_\gamma(\sigma) = [R_A^g(x, Q_{\text{eff}}^2)\theta(\sigma_0 - \sigma) + \theta(\sigma - \sigma_0)] P_\gamma(\sigma), \quad (7)$$

where  $x = Q_{\text{eff}}^2/W^2$  and  $P_\gamma(\sigma)$  is shown in Fig. 1 (left panel). The distribution  $P(\nu)$  corresponding to  $\sigma_\nu$  calculated using  $\tilde{P}_\gamma(\sigma)$  is given by the curve ‘‘Generalized CF’’ in the right panel of Fig. 1.

Finally, to test the importance of cross section (color) fluctuations in the real photon, we calculated  $P(\nu)$  neglecting these fluctuations and using

$$P_\gamma(\sigma) = \delta(\sigma - 25 \text{ mb}) \quad (8)$$

in Eq. (4). The result is given by the curve ‘‘Glauber’’ in Fig. 1. One can see from this figure that color fluctuations significantly increase the distribution  $P(\nu)$  at small and especially large  $\sigma$ ; the latter is emphasized in the insert.

In the total inelastic photon-nucleus cross section, the AGK cancellations manifest themselves as the observation that the average number of wounded nucleons  $\langle N_{\text{coll}} \rangle$  is inversely proportional to the nuclear shadowing factor. Generalizing the result of [34] for hadron-nucleus scattering to the case of photon-induced scattering, one obtains [26]

$$\langle N_{\text{coll}} \rangle \equiv \sum_{\nu=1}^A P(\nu)\nu = \frac{\sum_{\nu=1}^A \nu\sigma_\nu}{\sum_{\nu=1}^A \sigma_\nu} = \frac{A\sigma_{\text{inel}}^{\gamma N}}{\sigma_{\text{inel}}^{\gamma A}}, \quad (9)$$

where  $\sigma_{\text{inel}}^{\gamma N}$  is the photon-nucleon inelastic cross section. Considering a particular hard process in inelastic photon-nucleus scattering that probes the nuclear gluon distribution, e.g., inclusive charmonium (bottomonium) production  $\gamma + A \rightarrow J/\psi(\Upsilon) + X$  or inclusive heavy-quark dijet production  $\gamma + A \rightarrow QQ + X$ , one obtains using Eq. (9):

$$\langle N_{\text{coll}} \rangle \approx \frac{1}{R_{\text{Pb}}^g(x, Q^2)} \lesssim 2. \quad (10)$$

In this estimate we used the following considerations. In general, the effect of nuclear shadowing for the nuclear inelastic cross section is somewhat larger than that for the total cross section. However, the theoretical uncertainties of the leading twist approximation [9] largely mask the differences and make the shadowing effects approximately equal (within uncertainties) in the two cases. Finally, in the last step, we used the results of Eq. (2).

Figure 2 shows predictions of the leading twist approximation (LTA) for the average number of wounded nucleons  $\langle N_{\text{coll}} \rangle = 1/R_{\text{Pb}}^g(x, Q^2)$  in inelastic photon-nucleus (Pb) scattering as a function of  $x$  at  $Q^2 = 3, 20, \text{ and } 1000 \text{ GeV}^2$ . These values of  $Q^2$  correspond to photoproduction  $J/\psi$ ,  $\Upsilon$ , and high- $p_T$  dijets, respectively. One can see from the figure that in the discussed kinematics, the average number of wounded nucleons is modest. As a result, the series in Eq. (9) converges rather rapidly. In particular, we have checked that it is saturated by first six terms with a 5% precision. Note, however, that the convergence slows down in the limit of small  $x$ .

Measurements of  $\langle N_{\text{coll}} \rangle$  present a new method to study nuclear shadowing in inelastic photon-nucleus scattering. Unlike the observables used so far, the constraint of Eq. (10) indicates that one can perform a ‘‘Pomeron surgery’’ of nuclear shadowing by cutting a small number of Pomeron exchanges controlling the number of inelastic interactions with target nucleons. As a result, it gives an opportunity for an experimental determination of a small number of parameters quantifying nuclear shadowing, which leads to a systematic improvement of its theoretical description. We elaborate on it in the following section.

### III. THE DISTRIBUTIONS OVER THE NUMBER OF WOUNDED NUCLEON AND FORWARD NEUTRONS FROM NUCLEAR BREAKUP

The average number of inelastic interactions  $\langle N_{\text{coll}} \rangle$  encodes information on the energy and scale dependence of nuclear shadowing. To obtain a more microscopic description of nuclear shadowing, one needs to determine not only  $\langle N_{\text{coll}} \rangle$ , but also the entire distribution over the number of wounded nucleons. This can be done using experimental data on the neutron emission resulting from nucleus fragmentation in a given UPC process, e.g., in inclusive quarkonium or dijet photoproduction in heavy-ion UPCs with an additional condition of  $Xn$  neutrons in the zero degree calorimeter (ZDC) on the nuclear target side [18, 19].

Very little is known about the dynamics of neutron emission in high energy scattering off heavy nuclei. The ALICE collaboration measured the distribution over the number of collisions  $\langle N_{\text{coll}}(E_T) \rangle$  in proton-nucleus scattering as determined by the energy release ( $E_T$ ) at central rapidities and the neutron multiplicity as a function of  $E_T$  [45]. It

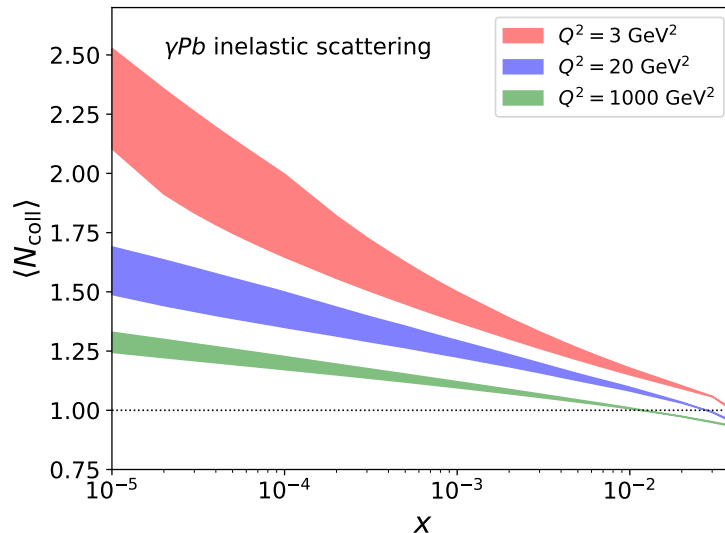


FIG. 2: The LTA predictions for the average number of wounded nucleons  $\langle N_{\text{coll}} \rangle$  in inelastic photon-nucleus (Pb) scattering as a function of  $x$  at  $Q^2 = 3, 20,$  and  $1000 \text{ GeV}^2$ .

was observed that  $\langle N_{\text{coll}}(E_T) \rangle$  is linearly proportional to the number of evaporation neutrons  $\langle M_n(E_T) \rangle$  for the same  $E_T$  bins at least up to  $\langle N_{\text{coll}} \rangle \sim 10$ . Note that in our case,  $\langle N_{\text{coll}} \rangle$  is much lower, see Eq. (10).

Another important observation made by the E665 experiment at Fermilab is that in muon-nucleus deep inelastic scattering (DIS) in coincidence with detection of slow neutrons,  $\mu^- + A \rightarrow n + X$ , the average neutron multiplicity  $\langle M_n \rangle$  for the lead target is [46]

$$\langle M_n \rangle \approx 5. \quad (11)$$

This result has been understood in the framework of cascade models of nuclear DIS [47, 48], where soft neutrons are produced either directly in DIS on a bound nucleon or through a statistical decay (de-excitation) of the excited residual nucleus, leading to neutron evaporation<sup>1</sup>. The latter mechanism depends strongly on the hadron formation time: to describe the energy spectrum of emitted neutrons, one has to assume that only nucleons and pions with momenta  $\leq 1 \text{ GeV}/c$  could be involved in final-state interactions. A similar conclusion was reached by M. Baker (private communication, 2022) using the BeAGLE Monte Carlo generator [50].

This suggests the following space-time picture of forward neutron production in high energy photon-nucleus scattering. Well before the target, the incoming photon fluctuates into long-lived hadronic components, which pass through the nucleus and interact inelastically with several nucleons. It leads to the creation of holes in the nucleus (particle-hole excitations in terminology of a nuclear shell model), which de-excite and cool the nucleus by evaporating neutrons. It also produces a number of soft particles with the momenta less than  $1 \text{ GeV}/c$ , which in turn generate more neutrons.

The nucleon fragmentation weakly depends on the incident energy due to Feynman scaling and, hence, it is not significantly affected by the energy conservation constraint, which is important in the case, when one uses hadron multiplicities at central rapidities [51]. In this case, the energy transferred to the rest of the nucleus, which heats the residual nuclear system, is proportional to  $\langle N_{\text{coll}} \rangle$ . Since the Fermilab data [46] corresponds to the average momentum fraction  $\langle x \rangle = 0.015$ , where the nuclear shadowing effect is small, one finds that  $\langle N_{\text{coll}} \rangle \approx 1$ , see Eq. (9). Thus, every inelastic photon-nucleon interaction results on average in 5 forward neutrons.

We use this hypothesis and perform the following numerical test study. First, we consider a simple model, which assumes that the probability density of neutron emission is given by the Poisson distribution and that each hole created in the target nucleus generates independently on average  $\langle M_n \rangle$  neutrons. Therefore, the neutron probability distribution for  $\nu = \langle N_{\text{coll}} \rangle$  wounded nucleons is

$$P_{\text{Poisson}}(N; \lambda = \nu \langle M_n \rangle) = \frac{(\nu \langle M_n \rangle)^N e^{-\nu \langle M_n \rangle}}{N!}, \quad (12)$$

<sup>1</sup> The geometry of the heating is very different from the case of AA collisions, where in each collision a large portion of nucleons in each nucleus interacts and de-excitation of the spectators only occurs close to the interaction surface [49].

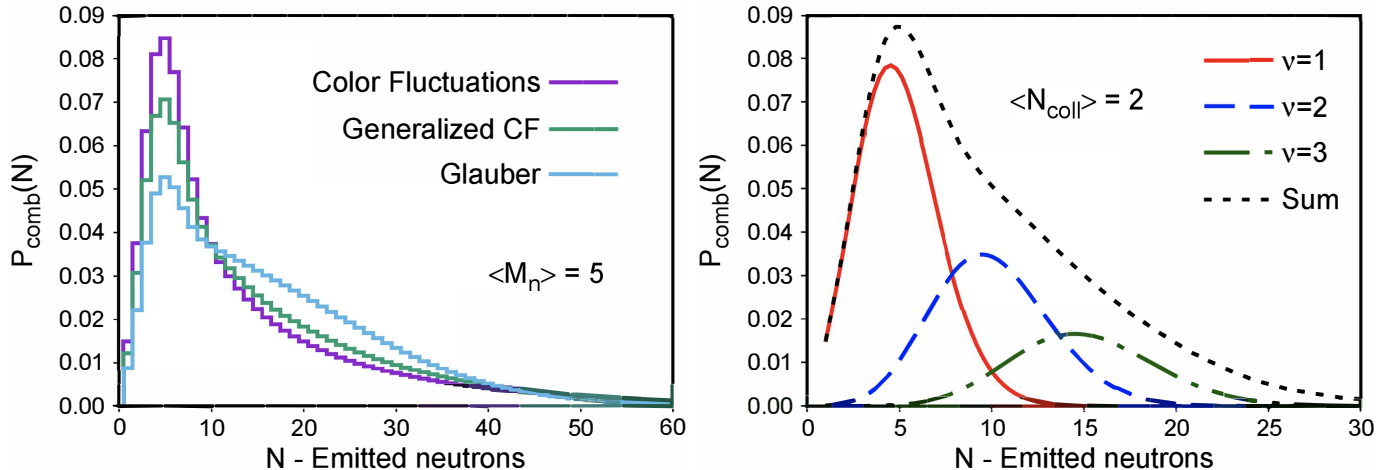


FIG. 3: (Left) The probability distribution of forward neutron emission  $P_{\text{comb}}(N)$  (13) as a function of the number of emitted neutrons  $N$  for  $\langle M_n \rangle = 5$ . The three curves correspond to the three models for  $P_\gamma(\sigma)$  discussed in text. (Right) The contributions of  $\nu = 1, 2, 3$  wounded nucleons to  $P_{\text{comb}}(N)$  in the Glauber model for  $P_\gamma(\sigma)$  chosen to correspond to  $\langle N_{\text{coll}} \rangle = 2$ . The black dotted curve labeled “Sum” gives the total  $P_{\text{comb}}(N)$ .

where  $N$  is the number of produced neutrons (neutron multiplicity).

Then, we combine the distribution over the number of wounded nucleons  $P(\nu)$  discussed in Sec. II with the Poisson distribution of produced neutrons (12). The resulting probability distribution of forward neutrons is given by the following expression,

$$P_{\text{comb}}(N) = \sum_{\nu=1}^A P(\nu) P_{\text{Poisson}}(N; \nu \langle M_n \rangle). \quad (13)$$

The left panel of Fig. 3 presents  $P_{\text{comb}}(N)$  as a function of forward neutrons  $N$  for  $\langle M_n \rangle = 5$ . The three curves correspond to the three models for the hadronic (color) fluctuations of the real photon, see the right panel of Fig. 1. One can see from the figure that cross section fluctuations of the real photon noticeably affect the shape of the neutron distribution: its maximum at small  $N$  is more pronounced compared to the “Glauber” result and is also somewhat suppressed by the leading twist shadowing in the “Generalized CF” case.

Extraction of the contributions of individual  $\nu$  (deconvolution) from the distribution  $P_{\text{comb}}(N)$  is feasible for not very large values of  $\sigma_{\text{inel}}^{\gamma N}$ . This is illustrated in the right panel of Fig. 3, which shows the contributions of  $\nu = 1, 2, 3$  wounded nucleons to  $P_{\text{comb}}(N)$  in the case, when  $P_\gamma = \delta(\sigma - \bar{\sigma})$  with  $\bar{\sigma}$  chosen to correspond to  $\langle N_{\text{coll}} \rangle = 2$ , see Fig. 2. The black dotted curve labeled “Sum” gives the total  $P_{\text{comb}}(N)$  in this model. One can see from the figure that the peaks of these contributions are sufficiently separated, which gives a principal possibility to reconstruct the distribution over wounded nucleons  $P(\nu)$ . Then one can use an iterative procedure to find individual  $\sigma_\nu$ . Indeed, assuming that the series in Eq. (3) of dominates by the  $\nu = 1, 2$  terms (the limit of weak nuclear shadowing), one obtains

$$\langle N_{\text{coll}} - 1 \rangle \approx \frac{\sigma_2}{\sigma_1} \approx \frac{A-1}{2} \frac{\langle \sigma_{\text{inel}}^2 \rangle}{\langle \sigma_{\text{inel}} \rangle} \int d^2\vec{b} T_A^2(\vec{b}), \quad (14)$$

where in the second equation, we used Eq. (4). The ratio  $\langle \sigma_{\text{inel}}^2 \rangle / \langle \sigma_{\text{inel}} \rangle$  plays a central role in the leading twist approach to nuclear shadowing, where it determines its magnitude in the weak shadowing limit. Working along these lines, one can determine higher moments  $\langle \sigma_{\text{inel}}^n \rangle / \langle \sigma_{\text{inel}} \rangle$ , see [52], which built up a full-fledged LTA shadowing correction.

The shape of the neutron distributions in Fig. 3 strongly depends on the magnitude of nuclear shadowing, which in turn is correlated with  $\langle N_{\text{coll}} \rangle$  and the  $x$ -dependence (energy dependence) of nuclear modification of nuclear PDFs in LTA: an increase of nuclear shadowing leads to the proportional increase of  $\langle N_{\text{coll}} \rangle$ , see Eq. (10) and Fig. 2, and, hence, to a wider distribution  $P_{\text{comb}}(N)$  with important contributions of large  $\nu$ . This is illustrated by the left panel of Fig. 4, which shows  $P_{\text{comb}}(N)$  as a function of  $N$  for  $\langle N_{\text{coll}} \rangle = 3$ . A comparison with the right panel of Fig. 3

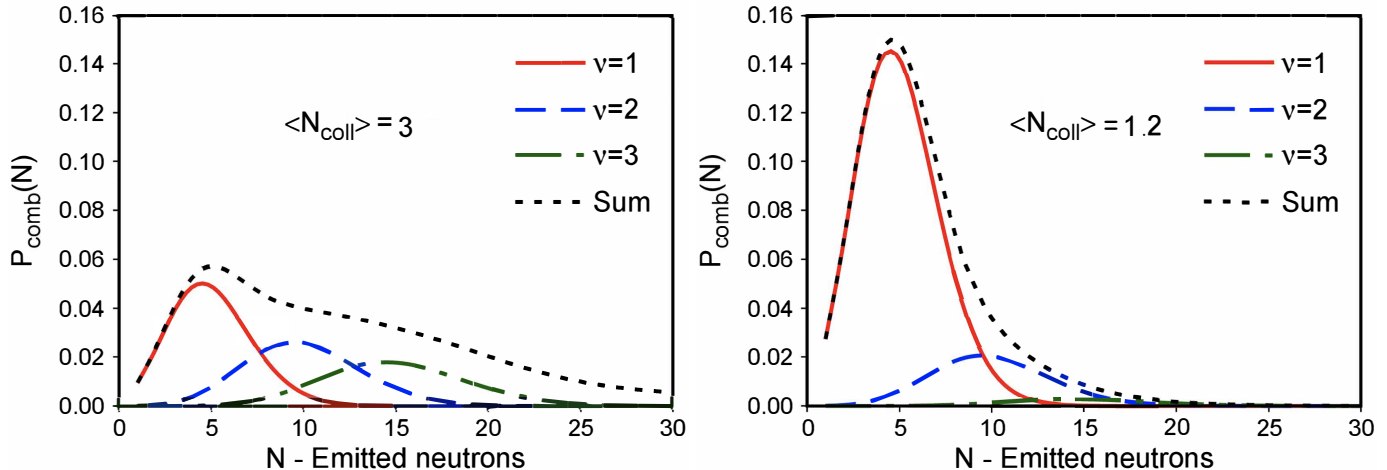


FIG. 4: The probability distribution of forward neutron emission  $P_{\text{comb}}(N)$  as a function of the number of emitted neutrons  $N$  for  $\langle M_n \rangle = 5$ . The left and right panels correspond to the strong nuclear shadowing with  $\langle N_{\text{coll}} \rangle = 3$  and weak shadowing with  $\langle N_{\text{coll}} \rangle = 1.2$ , respectively. See Fig. 3 for legend.

demonstrates that  $P_{\text{comb}}(N)$  has become wider (the black dotted curve) because of an important contribution of  $\nu \geq 2$  wounded nucleons.

Note that to reach a high accuracy in deconvolution of  $P_{\text{comb}}(N)$ , one needs to calibrate the theoretical description against the kinematics, where only one target nucleon is struck, e.g., using  $\gamma + A \rightarrow 2 \text{ jets} + X$  or quasi-elastic  $J/\psi$  production for  $x_A \geq 0.01$ , where the effect of nuclear shadowing is small and  $\langle N_{\text{coll}} \rangle \approx 1$ . It is supported by the results in the right panel of Fig. 4, which show that  $P_{\text{comb}}(N)$  at  $\langle N_{\text{coll}} \rangle = 1.2$  is dominated by the  $\nu = 1$  contribution.

In summary, an important qualitative effect predicted by our model is a strong increase of the multiplicity of neutrons detected in ZDCs with a decrease of  $x$  from  $x \sim 0.05$  corresponding to the right panel of Fig. 4, where nuclear shadowing is small, to  $x \sim 10^{-3}$  corresponding to the left panel of Fig. 4, where the shadowing effect is large. After measurements of the neutron multiplicity for large  $x$  are performed, it would be possible to test LTA predictions for the probabilities of 1, 2, 3 wounded nucleons as well as the assumption that emissions of neutrons generated by a removal of nucleons can be treated as independent.

#### IV. CONCLUSIONS AND OUTLOOK

In this paper, we suggest using measurements of forward neutrons from nuclear breakup in inclusive high energy photon-nucleus scattering in heavy-ion UPCs, e.g., charmonium (bottomonium) production  $\gamma + A \rightarrow J/\psi(\Upsilon) + X$  or heavy-quark dijet production  $\gamma + A \rightarrow Q\bar{Q} + X$ , as a novel way to study the QCD dynamics at small  $x$ . The key quantity is the number of inelastic photon-nucleon interactions (the number of wounded nucleons): its average value  $\langle N_{\text{coll}} \rangle$  is proportional to inverse of the gluon nuclear shadowing and its distribution is sensitive to details of nuclear shadowing. Our numerical analysis suggests that the number of forward neutrons from nuclear breakup detected in the ZDC on the nuclear target side is rather unambiguously proportional to the number of wounded nucleons, which provides a practical opportunity for novel studies of nuclear shadowing and its  $x$  dependence.

Using these processes, it would be possible to explore effects related to proximity to the black disk limit of the strong interaction. For example, one can study fragmentation of leading hadrons in  $\gamma A$  scattering and look for suppression of their multiplicity as a function of Feynman  $x_F$  and  $W$  as well as for broadening of their transverse momentum distribution [3]. These effects should be more pronounced for central collisions characterized by an enhanced activity in the ZDC. It should be possible to construct from the data an analog of the central-to-peripheral  $R_{CP}$  ratio of yields, which would probe the density dependence of fragmentation. It would also be useful to construct similar quantities for low- $p_T$  charm production.

Another interesting application is for multiparton interactions in proton-nucleus ( $pA$ ) scattering. It was argued in [53] that the single and double scattering can be separated using their dependence on the impact parameter: the former is proportional to  $A$ , while the latter  $\propto A^{4/3}$ . However, since both hard interactions are typically detected in a limited range of rapidities  $|y| \leq 3-4$ , centrality is difficult to determine from the transverse energy  $E_T$  signal because

multiparton interactions also contribute to  $E_T$ . The use of forward neutrons in ZDCs would alleviate this problem.

One should point out that the neutrons detected in ZDCs can be a promising complementary way to determine centrality of various photon-nucleus and proton-nucleus inelastic collisions expanding the use of ZDCs beyond their current use in vector meson diffractive production and for determining of centrality of the heavy-ion collisions. The main advantage of using forward neutrons rather than the transverse energy  $E_T$  for the determination of centrality is a much larger distance in rapidity between the rapidity of the hard process and that of the process used for determination of the centrality.

One of the principal problems of using UPCs for studies of small- $x$  phenomena is a lack of the nucleon reference data at similar energies with the precision necessary to observe nuclear effects with a better than 10% accuracy ( $J/\psi$  exclusive photoproduction is a notable exception). Below we outline a possible strategy for overcoming this problem. Note that we are not aiming to optimize cuts or to account for the energy resolution of ZDCs since this would require a dedicated Monte Carlo study.

One can separate events into two classes: peripheral events corresponding to  $\langle N_{\text{coll}} \rangle \leq 2$  (we call it class “L”) and more central events corresponding to  $\langle N_{\text{coll}} \rangle \geq 1.5 - 2$  and  $\langle M_n \rangle \sim 7 - 10$  (class “H”). If statistics is sufficient, the lower limit for class “H” can be gradually increased, which will push up the average number of wounded nucleons. Then, the ratio of the number of events in the two classes,  $\hat{R} = \text{Yield(H)}/\text{Yield(L)}$ , should quantify the effect of nuclear shadowing at small and large impact parameters, which in principle probes the dependence of nuclear shadowing on the thickness of nuclear matter. The promising channels for such an analysis include inclusive charm production with the transverse momentum in the range  $p_T = 5 - 20$  GeV/c and production of soft particles with small  $p_T < 0.5$  GeV/c. A comparison of the rates of these processes will allow one to study the transition between the soft and hard regimes and will serve as a consistency check of the description of small- $x$  dynamics in the current models.

The methods presented in this paper can be readily generalized to the case of virtual photons and allow one to predict the distribution over the number of forward neutrons in inelastic photon-nucleus scattering at the EIC.

### Acknowledgments

The research of V.G. was funded by the Academy of Finland project 330448, the Center of Excellence in Quark Matter of the Academy of Finland (projects 346325 and 346326), and the European Research Council project ERC-2018-ADG-835105 YoctoLHC. The research of M.S. was supported by the US Department of Energy Office of Science, Office of Nuclear Physics under Award No. DE-FG02-93ER40771.

- 
- [1] Y. L. Dokshitzer, D. Diakonov and S. I. Troian, Phys. Rept. **58**, 269-395 (1980)
  - [2] L. V. Gribov, E. M. Levin and M. G. Ryskin, Phys. Rept. **100**, 1-150 (1983)
  - [3] L. Frankfurt, V. Guzey, M. McDermott and M. Strikman, Phys. Rev. Lett. **87**, 192301 (2001) [arXiv:hep-ph/0104154 [hep-ph]].
  - [4] A. Accardi, J. L. Albacete, M. Anselmino, N. Armesto, E. C. Aschenauer, A. Bacchetta, D. Boer, W. K. Brooks, T. Burton and N. B. Chang, *et al.* Eur. Phys. J. A **52**, no.9, 268 (2016) [arXiv:1212.1701 [nucl-ex]].
  - [5] R. Abdul Khalek, A. Accardi, J. Adam, D. Adamiak, W. Akers, M. Albaladejo, A. Al-bataineh, M. G. Alexeev, F. Ameli and P. Antonioli, *et al.* Nucl. Phys. A **1026**, 122447 (2022) [arXiv:2103.05419 [physics.ins-det]].
  - [6] M. Strikman, R. Vogt and S. N. White, Phys. Rev. Lett. **96**, 082001 (2006) [arXiv:hep-ph/0508296 [hep-ph]].
  - [7] A. J. Baltz, G. Baur, D. d’Enterria, L. Frankfurt, F. Gelis, V. Guzey, K. Hencken, Y. Kharlov, M. Klasen and S. R. Klein, *et al.* Phys. Rept. **458**, 1-171 (2008)
  - [8] V. Guzey and M. Strikman, [arXiv:2404.17476 [hep-ph]].
  - [9] L. Frankfurt, V. Guzey and M. Strikman, Phys. Rept. **512**, 255-393 (2012) [arXiv:1106.2091 [hep-ph]].
  - [10] V. Guzey, E. Kryshen, M. Strikman and M. Zhalov, Phys. Lett. B **726**, 290-295 (2013) [arXiv:1305.1724 [hep-ph]].
  - [11] V. Guzey and M. Zhalov, JHEP **10**, 207 (2013) [arXiv:1307.4526 [hep-ph]].
  - [12] K. J. Eskola, C. A. Flett, V. Guzey, T. Löytäinen and H. Paukkunen, Phys. Rev. C **106**, no.3, 035202 (2022) [arXiv:2203.11613 [hep-ph]].
  - [13] K. J. Eskola, C. A. Flett, V. Guzey, T. Löytäinen and H. Paukkunen, Phys. Rev. C **107**, no.4, 044912 (2023) [arXiv:2210.16048 [hep-ph]].
  - [14] S. P. Jones, A. D. Martin, M. G. Ryskin and T. Teubner, J. Phys. G **43**, no.3, 035002 (2016) [arXiv:1507.06942 [hep-ph]].
  - [15] S. P. Jones, A. D. Martin, M. G. Ryskin and T. Teubner, Eur. Phys. J. C **76**, no.11, 633 (2016) [arXiv:1610.02272 [hep-ph]].
  - [16] V. Guzey and M. Klasen, Phys. Rev. C **99**, no.6, 065202 (2019) [arXiv:1811.10236 [hep-ph]].
  - [17] V. Guzey and M. Klasen, JHEP **04**, 158 (2016) [arXiv:1603.06055 [hep-ph]].
  - [18] [ATLAS], “Photo-nuclear dijet production in ultra-peripheral Pb+Pb collisions,” ATLAS-CONF-2017-011.



- [19] [ATLAS], “Photo-nuclear jet production in ultra-peripheral Pb+Pb collisions at  $\sqrt{s_{\text{NN}}} = 5.02$  TeV with the ATLAS detector,” ATLAS-CONF-2022-021.
- [20] B. Pire, L. Szymanowski and J. Wagner, Phys. Rev. D **79**, 014010 (2009) [arXiv:0811.0321 [hep-ph]].
- [21] W. Schafer, G. Slipek and A. Szczurek, Phys. Lett. B **688**, 185-191 (2010) [arXiv:1003.0610 [hep-ph]].
- [22] G. M. Peccini, L. S. Moriggi and M. V. T. Machado, Phys. Rev. D **103**, no.5, 054009 (2021) [arXiv:2101.08338 [hep-ph]].
- [23] S. R. Klein, J. Nystrand and R. Vogt, Phys. Rev. C **66**, 044906 (2002) [arXiv:hep-ph/0206220 [hep-ph]].
- [24] V. P. Goncalves, M. V. T. Machado and A. R. Meneses, Phys. Rev. D **80**, 034021 (2009) [arXiv:0905.2067 [hep-ph]].
- [25] V. P. Goncalves, G. Sampaio dos Santos and C. R. Sena, Nucl. Phys. A **976**, 33-45 (2018) [arXiv:1711.04497 [hep-ph]].
- [26] M. Alvioli, L. Frankfurt, V. Guzey, M. Strikman and M. Zhalov, Phys. Lett. B **767**, 450-457 (2017) [arXiv:1605.06606 [hep-ph]].
- [27] V. A. Abramovsky, V. N. Gribov and O. V. Kancheli, Yad. Fiz. **18**, 595-616 (1973), Sov. J. Nucl. Phys. **18**, 308-317 (1974).
- [28] D. Treleani, Int. J. Mod. Phys. A **11**, 613-654 (1996)
- [29] J. Jalilian-Marian and Y. V. Kovchegov, Phys. Rev. D **70**, 114017 (2004) [erratum: Phys. Rev. D **71**, 079901 (2005)] [arXiv:hep-ph/0405266 [hep-ph]].
- [30] F. Gelis and R. Venugopalan, Nucl. Phys. A **776**, 135-171 (2006) [arXiv:hep-ph/0601209 [hep-ph]].
- [31] A. Kovner and M. Lublinsky, JHEP **11**, 083 (2006) [arXiv:hep-ph/0609227 [hep-ph]].
- [32] N. N. Nikolaev and W. Schafer, Phys. Rev. D **74**, 074021 (2006) [arXiv:hep-ph/0607307 [hep-ph]].
- [33] L. Frankfurt and M. Strikman, Eur. Phys. J. A **5**, 293-306 (1999) [arXiv:hep-ph/9812322 [hep-ph]].
- [34] L. Bertocchi and D. Treleani, J. Phys. G **3**, 147 (1977)
- [35] A. Bialas, M. Bleszynski and W. Czyz, Nucl. Phys. B **111**, 461-476 (1976)
- [36] L. Frankfurt, V. Guzey, A. Stasto and M. Strikman, Rept. Prog. Phys. **85**, no.12, 126301 (2022) [arXiv:2203.12289 [hep-ph]].
- [37] K. A. Olive *et al.* [Particle Data Group], Chin. Phys. C **38**, 090001 (2014)
- [38] T. J. Chapin, R. L. Cool, K. A. Goulianos, K. A. Jenkins, J. P. Silverman, G. R. Snow, H. Sticker, S. N. White and Y. H. Chou, Phys. Rev. D **31**, 17-30 (1985)
- [39] M. Alvioli, B. A. Cole, L. Frankfurt, D. V. Perepelitsa and M. Strikman, Phys. Rev. C **93**, no.1, 011902 (2016) [arXiv:1409.7381 [hep-ph]].
- [40] M. Alvioli, L. Frankfurt, D. Perepelitsa and M. Strikman, Phys. Rev. D **98**, no.7, 071502 (2018) [arXiv:1709.04993 [hep-ph]].
- [41] D. V. Perepelitsa, [arXiv:2404.17660 [nucl-th]].
- [42] M. Alvioli, H. J. Drescher and M. Strikman, Phys. Lett. B **680**, 225-230 (2009) [arXiv:0905.2670 [nucl-th]].
- [43] M. Alvioli, C. Ciofi degli Atti, I. Marchino, V. Palli and H. Morita, Phys. Rev. C **78**, 031601 (2008) [arXiv:0807.0873 [nucl-th]].
- [44] M. Alvioli, C. Ciofi degli Atti and H. Morita, Phys. Rev. Lett. **100**, 162503 (2008)
- [45] S. Acharya *et al.* [ALICE], JHEP **08**, 086 (2022) [arXiv:2107.10757 [nucl-ex]].
- [46] M. R. Adams *et al.* [E665], Phys. Rev. Lett. **74**, 5198-5201 (1995) [erratum: Phys. Rev. Lett. **80**, 2020-2021 (1998)]
- [47] M. Strikman, M. G. Tverskoi and M. B. Zhalov, Phys. Lett. B **459**, 37-42 (1999) [arXiv:nucl-th/9806099 [nucl-th]].
- [48] A. B. Larionov and M. Strikman, Phys. Rev. C **101**, no.1, 014617 (2020) [arXiv:1812.08231 [hep-ph]].
- [49] M. Alvioli and M. Strikman, Phys. Rev. C **83**, 044905 (2011) [arXiv:1008.2328 [nucl-th]].
- [50] W. Chang, E. C. Aschenauer, M. D. Baker, A. Jentsch, J. H. Lee, Z. Tu, Z. Yin and L. Zheng, Phys. Rev. D **106**, no.1, 012007 (2022) [arXiv:2204.11998 [physics.comp-ph]].
- [51] G. Aad *et al.* [ATLAS], Eur. Phys. J. C **76**, no.4, 199 (2016) [arXiv:1508.00848 [hep-ex]].
- [52] M. Alvioli, L. Frankfurt, V. Guzey and M. Strikman, Phys. Rev. C **90**, 034914 (2014) [arXiv:1402.2868 [hep-ph]].
- [53] M. Alvioli, M. Azarkin, B. Blok and M. Strikman, Eur. Phys. J. C **79**, no.6, 482 (2019) [arXiv:1901.11266 [hep-ph]].